Indonesian Journal of Education & Mathematical Science
Vol. 7, No. 3, September 2026, pp. 363~375
ISSN: 2715-985X, DOI: 10.30596/ijems.v7i3.30962

A Data-Driven Travel-Time Scenario Framework for the Preliminary Analysis of School Meal Distribution as Education Support

Muliawan Firdaus[1], Marah Doly Nasution[2]
[1]Department of Mathematics, Universitas Negeri Medan, Medan, Indonesia
[2]Department of Mathematics Education, Universitas Muhammadiyah Sumatera Utara, Medan, Indonesia
[1]muliawanfirdaus@unimed.ac.id [2]marahdoly@umsu.ac.id

ABSTRACT

School meal distribution supports education, yet variable travel time makes delivery timing uncertain and can erode service reliability. This study builds a data-driven travel-time scenario framework for the preliminary screening of school meal distribution in Medan, Indonesia. The framework integrates school–depot nodes, OpenStreetMap road-network distance matrices processed with OSMnx, pilot TomTom traffic observations, and historical Open-Meteo weather profiles into a scenario travel-time matrix. Its focus is scenario-based travel-time risk screening rather than vehicle-route optimization or operational validation of official MBG/SPPG services, and the link between timeliness and educational outcomes is treated as conceptual motivation rather than a tested relationship. Results use a primary depot-to-school metric and a secondary all-OD network metric. Under the normal scenario, the mean depot-to-school travel time is 7.766 minutes; under a controlled extreme scenario it rises to 13.908 minutes, and the P90 increases from 11.044 to 19.779 minutes. The extreme scenario (S_5) is read as a conservative upper bound rather than a point estimate, because combining the traffic and weather factors risks double-counting. A sensitivity analysis shows a unit-elastic, inverse relationship between baseline speed and travel time. The framework offers an early computational representation of travel-time exposure in education-support school meal distribution.

Keywords: education-support logistics, pilot traffic observation, road-network distance, school meal distribution, travel-time scenario

Corresponding Author:
Muliawan Firdaus,
Department of Mathematics,
Universitas Negeri Medan,
Jalan Willem Iskandar Pasar V Medan Estate Medan 20221, Indonesia.
muliawanfirdaus@unimed.ac.id

1. INTRODUCTION

School meal programs are a form of education support, since attending to nutrition can shape learning readiness, attendance, and student wellbeing. A systematic review and meta-analysis by Wang *et al*. (2021) links school feeding in low- and middle-income countries to children's educational and health outcomes, yet finds those effects mixed across outcomes and stresses implementation quality and the need for stronger studies; we therefore treat the relationship as motivating background rather than a settled causal effect. Timing within that window matters as well: Cohen et al. (2016) found that the minutes children actually have to eat changed both what they chose and how much they finished. Seen this way, distribution is not simply moving food from place to place; it is one link in a wider education-support system whose payoff depends on governance, supply chains, and delivery that arrives when it should (Drake *et al*., 2016; Bundy *et al*., 2017; Bliznashka *et al*., 2024).

The path from timely distribution to learning runs through several steps: when travel time varies, meal arrival becomes uncertain, an uncertain arrival unsettles the meal schedule, and a disrupted schedule can then bear on intake and on how dependable the nutrition service is. This study engages only the first link. Measuring nutrient intake, concentration, attendance, or learning outcomes lies outside its scope, and the link to educational outcomes is kept conceptual rather than tested directly.

The Indonesian setting makes such analysis timely. The Free Nutritious Meal Program (*Program Makan Bergizi Gratis*, MBG) and its Nutrition Fulfillment Service Units (*Satuan Pelayanan Pemenuhan Gizi*, SPPG) are governed by technical guidelines from the National Nutrition Agency (*Badan Gizi Nasional*, BGN) under Decree No. 401.1 of 2025 (Badan Gizi Nasional, 2025a), with food-safety certification for SPPG set out in Decree No. 52.2 of 2025 (Badan Gizi Nasional, 2025b), together covering menu provision, governance, compliance, and food safety. In a release dated 31 May 2026, BGN reported that between 6 January 2025 and 29 May 2026, of 27,208 SPPG in operation, 8,182 had

Vol. 7, No. 3, September 2026, pp. 363~375
ISSN: 2715-985X, DOI: 10.30596/ijems.v7i3.30962

been temporarily suspended at some point and 2,213 remained suspended (Badan Gizi Nasional, 2026). We use these figures as policy context, not as analytical data.

Urban planning needs travel-time estimates that go beyond straight-line distance, because vehicles move through a road network shaped by connectivity, intersections, obstructions, and conditions that change over time; the time-dependent vehicle-routing literature shows that both traffic and departure time alter travel time (Malandraki & Daskin, 1992; Ichoua *et al*., 2003; Gendreau *et al*., 2015; Blauth *et al*., 2022). Gajpal *et al*. (2019), studying mid-day meal distribution in India, treat the task as route optimization with delivery ahead of the eating schedule, whereas our aim is earlier: to estimate travel-time exposure from the road network, pilot traffic, and historical weather before any optimization. Methodologically we take a middle path between simple distance-based estimation and full real-time prediction. OSMnx supports reproducible OpenStreetMap road networks (Boeing, 2017, 2022, 2025); related OpenStreetMap work has computed reproducible origin-destination distances and times through a different engine, OSRM (Huber & Rust, 2016), which we cite as context rather than conflate with our pipeline. Since a static network carries no traffic, we add pilot TomTom observations as a scenario traffic-correction factor and Open-Meteo historical weather (Acharya *et al*., 2024; TomTom, 2025; Open-Meteo, 2026), following the practice of estimating travel time from limited open data when fleet-operational data are unavailable (Boeing & Zhou, 2026; Ludwig *et al*., 2023), whose authors also warn that a naïve maximum- or constant-speed assumption tends to under-predict travel time, a caution that bears on the constant-speed model used here.

The gap is narrow and deliberate: no simple, open, and reproducible framework yet merges road-network distance, pilot traffic, and historical weather into a preliminary-screening scenario travel-time matrix for school meal distribution in a developing city where fleet data are unavailable. Each component is included because it captures a distinct source of travel-time variation: road-network distance sets the spatial structure of feasible movement but assumes free-flow conditions, pilot TomTom observations add an empirical correction for temporal congestion, and historical Open-Meteo profiles represent weather conditions that can further lengthen travel time. Combining the three is necessary because distance-only estimation tends to underestimate travel-time exposure, while full fleet telemetry is not feasible where operational fleet data are unavailable. Both Gajpal *et al*. (2019) and the WFP Route the Meals initiative (World Food Programme Innovation Accelerator, 2026) carry out real route optimization, the latter reportedly cutting lead time, distance, and emissions in the field; our framework sits one stage earlier and does not compete at that level, so we cite Route the Meals for positioning rather than as a quantitative benchmark. The contribution is a data-driven travel-time scenario framework comprising a node representation of depot and schools, a road-network distance matrix as the spatial basis, a traffic factor from pilot TomTom data, a weather factor from Open-Meteo, a set of normal, pilot-traffic, rainy, severe-congestion, and controlled-extreme scenarios with a non-composite comparator, and a sensitivity analysis on the baseline-speed parameter. We position it as preliminary travel-time risk screening, not an operational digital twin, an operational validation of MBG/SPPG, a food-safety model, or a final route-optimization model.

2. RESEARCH METHOD

A. Research Design

The study uses a computational design based on secondary data and API observations. This design is transparent, reproducible, and relatively economical, since it builds a consistent origin-destination matrix from open data and API observations without requiring proprietary fleet telemetry. It can also be updated as new observations become available and lets several scenarios be tested without intervening in actual school-meal operations. The TomTom observations are used only as a pilot traffic correction rather than a full multi-day profile. The method proceeds through node definition, construction of the road-network distance matrix, formulation of base travel time, construction of the pilot traffic factor, construction of the weather factor, scenario design, construction of the scenario travel-time matrix, sensitivity analysis, and a reproducibility statement.

B. Data Sources and Analytical Roles

The data are positioned as simulative analytical components for building the travel-time scenario framework. They support a reading of travel-time risk exposure in the school meal distribution system

Indonesian Journal of Education & Mathematical Science
Vol. 7, No. 3, September 2026, pp. 363~375
ISSN: 2715-985X, DOI: 10.30596/ijems.v7i3.30962

while remaining distinct from official MBG/SPPG operational records. Table 1 sets out the data sources and their analytical functions.

C. Nodes, Road Network, and Base Travel Time

C. Nodes, Road Network, and Base Travel Time

Let $\mathcal{V}$ be the full node set, comprising the depot and the schools, with $\mathcal{N}$ denote the set of schools and the depot fixed as node 0.

$$\mathcal{V} = \{0\} \cup \mathcal{N}, \qquad \mathcal{N} = \{1,2,\dots,n\} \tag{1}$$

Table 1. Data Sources and Analytical Roles in the Travel-Time Scenario Framework

Data component	Data type	Main variables	Function in the framework	Limitation
School and depot nodes	Coordinate data	District, status, student proxy, latitude, longitude	Define service nodes	Simulative, not official MBG/SPPG data
Road-network distance matrix	OD matrix	L_{ij}	Basis for estimating T_{ij}^0	Static; does not yet carry traffic
TomTom observations	Pilot traffic observations	CS_p, FFS_p, CTT_p, $FFTT_p$, α_p	Form the scenario traffic factor	Not a multi-day profile
Open-Meteo weather data	Historical weather	Precipitation, rain class, β_t	Form the scenario weather factor	Not food/cabin temperature
Scenario travel-time matrix	Derived data	T_{ij}^h, θ_h	Compare scenarios S_1-S_5	No route optimization yet

Distances come from the OSMnx road-network distance matrix rather than from Euclidean distance, where L_{ij} (km) is the road-network distance from node i to node j. Base travel time then follows from a baseline speed v_0 in km/h (Ludwig *et al*., 2023):

$$T_{ij}^0 = \frac{L_{ij}}{v_0} \times 60 \tag{2}$$

with T_{ij}^0 in minutes. We set $v_0 = 30$ km/h as a uniform baseline assumption for an initial estimate under normal conditions, not as a validated field speed. Structurally this is a "naive" constant-speed model in the sense of Boeing & Zhou (2026), who find that naïve maximum-speed prediction tends to under-predict true travel time by more than three minutes on average in their case study. The normal-scenario (S_1) estimates may therefore run optimistically low, so the absolute S_1 values are best read as an indicative lower bound; the scenario multiplier θ_h offsets this only in part and does not replace field calibration. Sincev_0 governs the results so strongly, we test the model's sensitivity to its variation.

We use OSM as the working basis for distance because it lends itself to graph-based modeling, though we have not checked its completeness for Medan against official local road records. That no OD pair came back disconnected tells us only that the graph is connected, not that the network is complete. A firmer adequacy check is left for later work, looking at edge density, the spread of segment lengths, and node degree, and spot-checking sample routes against an independent mapping service.

D. Pilot TomTom Traffic Factor

Let $\mathcal{P}$ be the set of TomTom monitoring points. At each point $p \in \mathcal{P}$ we form the traffic factor as the ratio of the observed travel time to the free-flow travel time at that same point.

$$\alpha_p = \frac{CTT_p}{FFTT_p} \tag{3}$$

Here CTT_p is the current travel time and $FFTT_p$ the free-flow travel time at p, in the sense the TomTom Flow Segment Data API uses these terms; for completeness the results tables also list the current speed CS_p and free-flow speed FFS_p. We work with a time ratio rather than a speed ratio because travel time is exactly what the framework outputs, and such a ratio is bounded below by one whenever traffic runs from normal to congested ($\alpha_p \geq 1$).

Taken together these ratios give a single pilot snapshot across the ten monitoring points rather than a continuous record, and we log the retrieval timestamp so the same pull can be repeated. Two caveats apply: the local weather state at retrieval was not checked against field weather sensors, so α_p may already absorb part of the weather effect, and each value reflects the road segments around a monitoring point rather than the full travel time of an OD route. We therefore read α_p as a pilot scenario factor, not a multi-day empirical traffic profile or a complete representation of traffic in Medan. The median of the TomTom factors drives the pilot-traffic scenario and the 90th percentile the severe-congestion scenario:

$$\alpha_{S_2} = \mathrm{median}(\alpha_p), \qquad \alpha_{S_4} = P_{90}(\alpha_p) \tag{4}$$

E. Weather Factor

The weather factor β_t classifies precipitation over the distribution window; its rain thresholds act as operational scenario cut-offs, not as an official climatological classification:

$$\beta_t = \begin{cases} 1.00, & \text{if dry or no rain,} \\ 1.05, & \text{if light rain } (0 < p \leq 1 \text{ mm/h}), \\ 1.10, & \text{if moderate rain } (1 < p \leq 4 \text{ mm/h}), \\ 1.20, & \text{if heavy rain or storm } (p > 4 \text{ mm/h}). \end{cases} \tag{5}$$

Rain is known to alter travel time, speed, and urban traffic intensity (Maze *et al*., 2006; Cools *et al*., 2010; Tsapakis *et al*., 2013), which supports the ordinal form used here, the multiplier grows with rainfall intensity. That literature does not, however, fix the specific values $1.05/1.10/1.20$, so we state plainly that the β_t are assumed parameters rather than the result of local calibration for Medan; their influence should be judged alongside the sensitivity analysis and the non-composite comparator, with field calibration left to future work. The scenario weather factor is taken as the maximum over the distribution window $\mathcal{T}_d$:

$$\beta_h = \max_{t \in \mathcal{T}_d} \beta_t \tag{6}$$

F. Scenario-Multiplier Design and the Double-Counting Risk

Scenario travel time applies a total multiplier θ_h to the base time:

$$T_{ij}^h = T_{ij}^0 \times \theta_h \tag{7}$$

For the main scenarios the multiplier is composite:

$$\theta_h = \alpha_h \beta_h \tag{8}$$

Eq. (8) acts as a controlled scenario multiplier, not as a causal model establishing independence between traffic and weather. Because the weather state at the time of the TomTom observations was not independently verified, an α_h that already embeds a rain effect would make the product $\alpha_h \beta_h$ count rain twice (double-counting). For that reason the composite scenarios, and S_5 in particular, are labeled as conservative upper-bound screening scenarios rather than point estimates or daily empirical predictions.

Where the weather-traffic interaction cannot be verified, a non-composite alternative serves as a sensitivity comparator:

$$\tilde{\theta}_h = \max(\alpha_h, \beta_h) \tag{9}$$

Eq. (9) does not combine the two effects multiplicatively, so it is more conservative against double-counting. Our headline numbers keep the composite form of Eq. (8) and should be read as no more than an early scenario reading; for S_5 we set the non-composite value beside it so the two can be compared directly. The five scenarios are:

$$S = \{S_1, S_2, S_3, S_4, S_5\} \tag{10}$$

with traffic factors:

Indonesian Journal of Education & Mathematical Science
Vol. 7, No. 3, September 2026, pp. 363~375
ISSN: 2715-985X, DOI: 10.30596/ijems.v7i3.30962

$$\alpha_h = \begin{cases} 1.0000, & h = S_1, \\ 1.2927, & h = S_2, \\ 1.0000, & h = S_3, \\ 1.3567, & h = S_4, \\ 1.20 \times 1.3567 = 1.6281, & h = S_5, \end{cases} \tag{11}$$

and weather factor:

$$\beta_h = \begin{cases} 1.0000, & h \in \{S_1, S_2, S_4\}, \\ 1.1000, & h \in \{S_3, S_5\}. \end{cases} \tag{12}$$

The value $\alpha_{S_5} = 1.6281$ uses the full-precision $P90(\alpha_p) \approx 1.35673$, so that $1.20 \times 1.35673 \approx 1.6281$; the four-decimal value 1.3567 would instead give 1.6280. Every later computation carries full precision, so this ± 0.0001 gap leaves the rounded entries in Table 5 untouched. The controlled-extreme multiplier for S_5 is therefore:

$$\theta_{S_5} = \alpha_{S_5}\beta_{S_5} = (1.20 \times 1.3567) \times 1.1000 = 1.7909 \tag{13}$$

We express each scenario's effect as its percentage change against the normal baseline:

$$\Delta_h = \frac{\overline{T}^h - \overline{T}^{S_1}}{\overline{T}^{S_1}} \times 100\% \tag{14}$$

G. Analysis Metrics

We keep two travel-time statistics apart throughout. The depot-to-school statistic is the primary one, since the service we model runs from a single depot out to the schools. The all-OD-pairs statistic is secondary: it describes the general travel-time structure among the nodes rather than the service itself. So the two are never confused, every figure in the Results carries an explicit label, "depot-to-school" or "all-OD." The depot-to-school pairs are:

$$\mathcal{D} = \{(0, i) \mid i \in \mathcal{N}\} \tag{15}$$

The mean depot-to-school travel time under scenario h is:

$$\overline{T}_{0\mathcal{N}}^h = \frac{1}{|\mathcal{N}|} \sum_{i \in \mathcal{N}} T_{0i}^h \tag{16}$$

For the all-valid-OD statistic, let $\mathcal{E}$ collect every valid OD pair, leaving out the diagonal and any pair flagged as disconnected. The mean travel time across these pairs is:

$$\overline{T}_{\mathcal{E}}^h = \frac{1}{|\mathcal{E}|} \sum_{(i,j) \in \mathcal{E}} T_{ij}^h \tag{17}$$

We attach a student-count proxy to each node only to convey the scale of service it represents. Since the scenarios deal in travel time and not in portion counts, vehicle capacities, or capacitated routes, this proxy never enters the travel-time model as a demand quantity.

H. Sensitivity Analysis

For any scenario with a fixed multiplier θ_h, the mean travel time takes the closed form:

$$\overline{T}^h = \frac{60 \cdot \overline{L} \cdot \theta_h}{v_0} \tag{18}$$

Differentiating with respect to the baseline speed v_0 gives:

$$\frac{\partial \overline{T}^h}{\partial v_0} = -\frac{60 \cdot \overline{L} \cdot \theta_h}{v_0^2} = -\frac{\overline{T}^h}{v_0} \tag{19}$$

From this, the elasticity in v_0 works out to:

$$\varepsilon_{v_0} = \frac{\partial \overline{T}^h / \overline{T}^h}{\partial v_0 / v_0} = -1 \tag{20}$$

If a scenario follows the multiplicative branch $\theta_h = \alpha_h \beta_h$, the elasticities with respect to α_h and β_h are likewise unit-elastic:

$$\varepsilon_\alpha = +1, \qquad \varepsilon_\beta = +1 \tag{21}$$

Indonesian Journal of Education & Mathematical Science
Vol. 7, No. 3, September 2026, pp. 363~375
ISSN: 2715-985X, DOI: 10.30596/ijems.v7i3.30962

Eq. (20) and (21) hold for the scalar model used here and nowhere beyond it. The unit elasticity $\varepsilon_{v_0} = -1$ is a property of that algebra, not a law of urban traffic: once volume approaches a road's critical capacity, the ties among speed, volume, queueing, and travel time can turn nonlinear in ways the scalar form does not capture. We therefore read the sensitivity results as a guide to how parameter uncertainty travels through an early framework, not as a replacement for a fuller dynamic traffic model.

I. Reproducibility

The run writes out its analysis tables, figures, processed data, the scenario travel-time matrix, the configuration file, and procedure logs, and these together act as replication material for the manuscript. The same record holds the TomTom retrieval metadata (timestamp and access date), the baseline-speed setting, the scenario factors, the decimal precision behind each multiplier, and notes on how the data were processed.

3. RESULTS AND DISCUSSION

A. Characteristics of the School Service Nodes

The node set is one simulative depot together with 99 schools. For each school we hold its district, status, coordinates, a student-count proxy, and its initial distance to the depot. These nodes are simulative; they stand in for service points and are not drawn from official MBG recipient lists or live SPPG operations. Because the proxy is built by spreading per-district reference figures by weight, some schools carry non-integer student counts. To keep the article compact, Table 2 reports the nodes aggregated to district level.

Table 2. Summary of School Service Nodes by District

District	No. of schools	Total student proxy	Mean student proxy	Mean distance to depot (km)	Max. distance to depot (km)
Medan Amplas	9	3,645	405.000	3.636	5.550
Medan Barat	4	1,767	441.750	4.997	5.460
Medan Baru	8	1,596.035	199.504	5.386	5.650
Medan Denai	15	4,138.035	275.869	3.937	5.280
Medan Kota	32	6,556.017	204.876	2.779	5.510
Medan Maimun	11	3,567	324.273	3.837	5.810
Medan Petisah	4	321.051	80.263	4.895	5.480
Medan Polonia	10	1,791	179.100	4.542	5.800
Medan Timur	6	1,950	325.000	5.263	5.790

As Table 2 and Fig 1 show, the service nodes spread unevenly across nine districts: Medan Kota carries the most, followed by Medan Denai. That imbalance matters for distribution, since the busier districts are likely to concentrate demand, even though we do not yet optimise the order in which vehicles visit them.

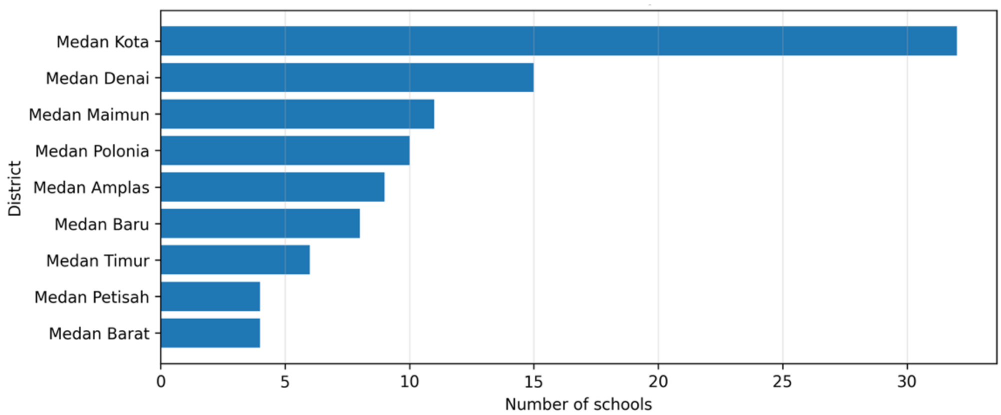

Fig 1. Distribution of School Service Nodes by District

Indonesian Journal of Education & Mathematical Science
Vol. 7, No. 3, September 2026, pp. 363~375
ISSN: 2715-985X, DOI: 10.30596/ijems.v7i3.30962

B. Road-Network Distance Statistics

The inter-node distance matrix is used to compute road-network distances. Where it appears, a value of 9999.0 marks a disconnected origin-destination pair and is excluded from the valid statistics. The value 9999.0 is not a distance threshold taken from the literature but a sentinel code assigned within the data-processing procedure. It is written whenever the shortest-path search returns no finite route between an origin and a destination, that is, when the two nodes are not connected on the routable road network. Because it does not represent an observed distance, it is excluded from all valid-distance and travel-time statistics. Table 3 reports the distance-matrix validation.

Four OD pairs with $L_{ij} = 0.000$ km are excluded from the scenario analysis because two nodes share the same nearest OSMnx network point. Removing these four pairs corresponds to about 0.04% of the total OD pairs (4/9900) and does not materially change the distribution. The off-diagonal count of 9,900 is consistent with 100×99, and the effective count is $9{,}896 = 9{,}900 - 4$.

Table 3. Road-Network Distance Statistics

Indicator	Value
Number of row nodes	100
Number of column nodes	100
Off-diagonal OD pairs	9,900
Topologically valid OD pairs	9,900
Disconnected OD pairs 9999.0	0
OD pairs effective for scenarios	9,896
Mean distance, all valid OD (km)	4.966
Median distance, all valid OD (km)	4.927
P90 distance, all valid OD (km)	7.881
Maximum distance, all valid OD (km)	11.571
Mean depot-to-school distance (km)	3.883
Median depot-to-school distance (km)	4.131
P90 depot-to-school distance (km)	5.522
Maximum depot-to-school distance (km)	6.219

Table 3 and the distance distribution in Fig 2 bring out an important difference between the all-OD statistic and the depot-to-school statistic. The mean distance across all valid OD pairs reaches 4.966 km, whereas the mean depot-to-school distance is 3.883 km. For that reason, the main distribution-service results are read through the depot-to-school statistic, with the all-OD statistic serving as a secondary network picture.

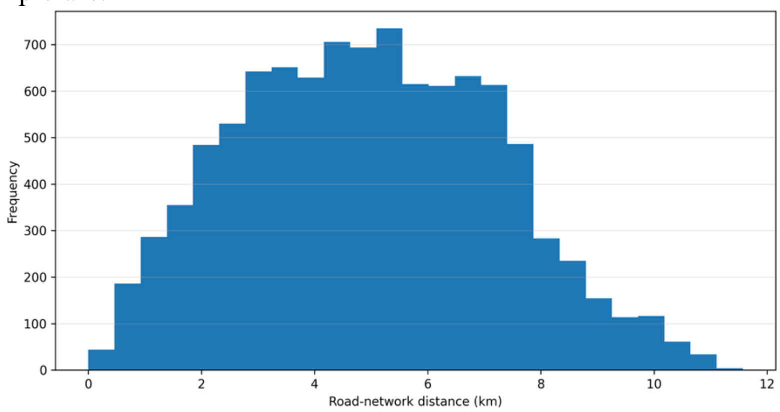

Fig 2. Distribution of Road-Network Distances

Indonesian Journal of Education & Mathematical Science
Vol. 7, No. 3, September 2026, pp. 363~375
ISSN: 2715-985X, DOI: 10.30596/ijems.v7i3.30962

C. External Scenario Parameters: TomTom and Open-Meteo

To keep the presentation compact, we combine the summary of TomTom observations and the weather profiles into a single set of external scenario parameters. TomTom forms the traffic factor and Open-Meteo the weather factor. Table 4 sets out the scenario parameters used in the travel-time computation.

We note that the TomTom observations are a pilot snapshot across 10 monitoring points. The execution log records the TomTom retrieval timestamp and provides reproducibility information. The weather state at the time of TomTom retrieval has not been independently verified. The composite scenario S_5 is therefore labeled an upper-bound screening scenario (a conservative upper bound), not the primary empirical prediction.

Table 4. External Scenario Parameters and Travel-Time Multipliers

Scenario	Scenario name	Traffic-factor basis	α_h	Weather-factor basis	β_h	θ_h	Interpretation
S_1	Normal baseline	No traffic penalty	1.0000	Dry conditions	1.0000	1.0000	Base condition
S_2	Pilot TomTom traffic	Median α_p over 10 TomTom points	1.2927	Dry conditions	1.0000	1.2927	Pilot-traffic scenario
S_3	Rainy weather	No traffic penalty	1.0000	Max. rain factor over the distribution window	1.1000	1.1000	Rainy scenario
S_4	Severe congestion	$P_{90}(\alpha_p)$ over 10 TomTom points	1.3567	Dry conditions	1.0000	1.3567	Traffic stress test
S_5	Controlled extreme stress	$1.20 \times P_{90}(\alpha_p)$	1.6281	Max. rain factor over the distribution window	1.1000	1.7909	Conservative upper bound

Table 4 and Fig 3 show that the pilot traffic factor is larger than the moderate-rain weather factor. The values $\alpha_{S_2} = 1.2927$ and $\alpha_{S_4} = 1.3567$ indicate that the TomTom observations capture a rise in travel time relative to free-flow conditions at the monitoring points. The value $\beta_h = 1.1000$, meanwhile, represents the moderate weather penalty used for the rainy scenario (Sakhare *et al.*, 2023; Xiong *et al.*, 2022). Combining the two in S_5 calls for cautious reading, because the traffic and weather effects may overlap.

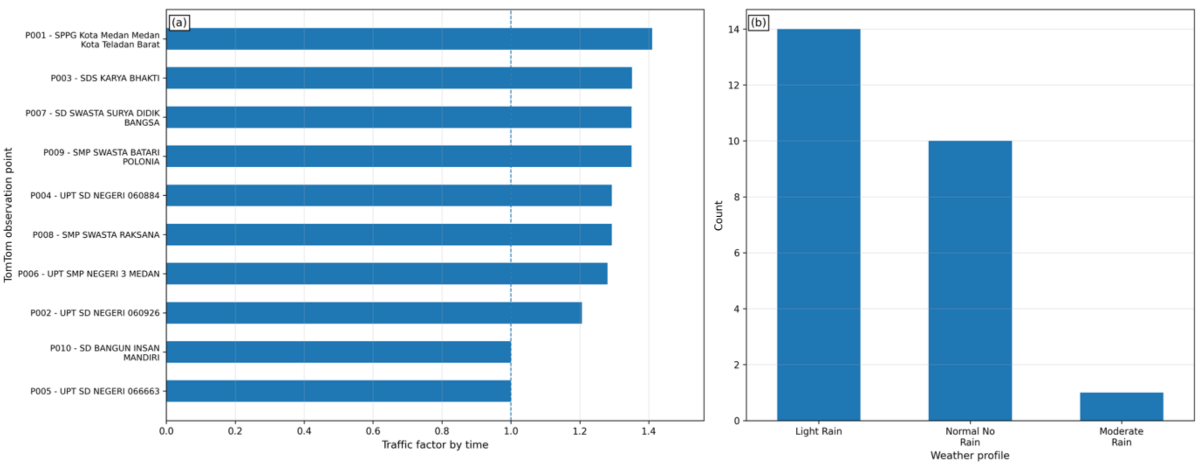

Fig 3. (a) Pilot TomTom Traffic Factor by Monitoring Point; (b) Weather Profiles over the Distribution Window

Indonesian Journal of Education & Mathematical Science
Vol. 7, No. 3, September 2026, pp. 363~375
ISSN: 2715-985X, DOI: 10.30596/ijems.v7i3.30962

D. Main Results: Depot-to-School Travel Time

Because the service runs from a single depot to schools, the main results use the depot-to-school statistic. Table 5 reports travel time for the five scenarios. All values are depot-to-school statistics, and they scale directly with θ_h. The mean rises from 7.766 minutes under the normal scenario (S_1) to 13.908 minutes under the controlled-extreme scenario (S_5), and P90 from 11.044 to 19.779 minutes (Fig 4), showing that the traffic and weather factors enlarge distribution-time exposure, most of all for schools in the upper tail of the distance distribution.

S_5 is meant as a conservative ceiling, not a prediction for any single day. If the TomTom factor already carries part of the rain signal, multiplying it by the weather factor in the composite $\theta_{S5} = \alpha_{S5}\beta_{S5}$would count that rain twice and overstate the combined impact. A non-composite comparator $\theta_{S5} = \max(\alpha_{S5}, \beta_{S5}) = \max(1.6281,\ 1.1000) = 1.6281$ gives a mean of $7.766 \times 1.6281 = 12.644$minutes and a P90 of $11.044 \times 1.6281 = 17.981$minutes. From S_1 through S_4 only one factor is ever active, so the composite and non-composite multipliers coincide and the comparator changes nothing there; it bears on S_5 alone. The band this opens for S_5 (12.644 minutes, non-composite) against 13.908 minutes (composite), is how we keep the double-counting risk in plain view.

Table 5. Depot-to-School Travel-Time Results by Scenario

Scenario	Scenario name	θ_h	Mean (min)	Median (min)	P90 (min)	Max. (min)	Mean increase from S_1
S_1	Normal baseline	1.0000	7.766	8.262	11.044	12.438	0.00%
S_2	Pilot TomTom traffic	1.2927	10.039	10.680	14.276	16.078	29.27%
S_3	Rainy weather	1.1000	8.543	9.088	12.148	13.682	10.00%
S_4	Severe congestion	1.3567	10.537	11.209	14.984	16.875	35.67%
S_5	Controlled extreme stress	1.7909	13.908	14.796	19.779	22.275	79.09%

For a planner, the use of these figures is in pointing to the schools that deserve a closer look, in when their vehicles should depart, whether an intermediate drop-off would help, or whether a backup vehicle should be held in reserve.

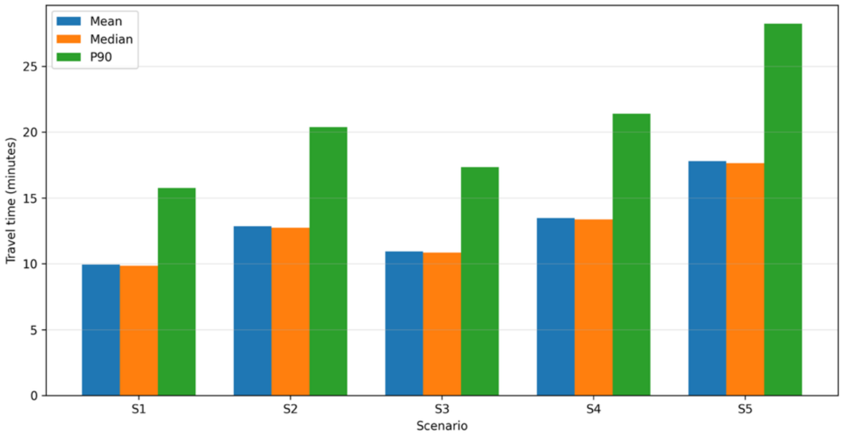

Fig 4. Comparison of Depot-to-School Travel Time by Scenario

Read at the network level (all-OD) instead, the mean travel time climbs from 9.935 minutes at S_1 to 17.793 minutes at S_5, and the P90 from 15.763 to 28.230 minutes. These all-OD figures are higher than the depot-to-school figures because they include school-to-school trips that are not always relevant as primary service journeys. The all-OD statistic is therefore used to read network structure, not as a direct indicator of depot-to-school distribution performance. The effective speed under the extreme scenario for all OD pairs is:

$$v_{\mathrm{eff},S_5} = \frac{\overline{L}_{\mathcal{E}}}{\overline{T}_{\mathcal{E}}^{S_5}/60} = \frac{4.966}{17.793/60} \approx 16.75 \text{ km/h} \tag{22}$$

This equals $v_0/\theta_{S_5} = 30/1.7909 \approx 16.75$ km/h and indicates that the controlled-extreme scenario implies a drop in the network's effective speed to about 16.75 km/h, averaged over all valid OD pairs.

E. Sensitivity to the Baseline Speed

We run the sensitivity analysis over $v_0 \in \{25,30,35,40\}$ km/h. On the all-valid-OD statistic, when $v_0 = 25$ km/h the mean S_1 travel time rises to 11.922 minutes and the mean S_5 travel time to 21.352 minutes. When $v_0 = 40$ km/h, the mean S_1 travel time falls to 7.451 minutes and the mean S_5 to 13.345 minutes. Both movements track the scalar relationship set out in Eq. (18)-(20).

This sensitivity asks to be read with care. The unit relationship $\varepsilon_{v_0} = -1$ falls straight out of the form $\overline{T}^h = 60\overline{L}\theta_h/v_0$: change v_0 by some fraction and travel time shifts by the same fraction in the opposite direction. Real urban traffic is not so tidy, speed responds to vehicle volume, road capacity, intersections, queueing, and local disturbances, none of which the scalar form sees. Holding speed fixed at $v_0 = 30$ km/h can moreover under-state real travel time (Boeing & Zhou, 2026), which is just what the v_0 sweep is there to probe: how far the estimates move if the true field speed is lower. We use it to read the model's internal structure, then, not to stand in for a macroscopic traffic model or a dynamic simulation.

F. Implications for Education-Support Logistics

The framework can flag risk exposure in school meal distribution before full operational data exist, since delivery delay may conceptually disrupt the stability of meal schedules and since meal duration and scheduling are known to relate to student consumption (Cohen *et al*., 2016); because the study does not directly test intake, concentration, attendance, or learning, we treat the link to educational outcomes as a conceptual motivation, the more so as the meta-analytic evidence is mixed and contingent on implementation quality (Wang *et al*., 2021), so the educational contribution lies in offering an early instrument for reading logistical risk rather than in proving educational impact. Practically, the depot-to-school P90 values in Table 5 identify the upper-tail schools that planners can prioritize in service-zone planning, departure scheduling, the choice of intermediate distribution points, or the provision of extra vehicles, and these can later be tied to data on vehicle capacity, school service times, actual arrival times, and food temperature. More broadly, WFP Route the Meals shows that school meal systems benefit from fuller distribution-network analysis once operational data, fleet capacity, and vehicle routes are available (World Food Programme Innovation Accelerator, 2026), and Gajpal *et al*. (2019) present a route-optimization formulation for mid-day meal delivery, whereas this study sits at an earlier stage, screening travel-time risk from scenarios and open data as a basis for moving toward route optimization in subsequent work.

G. Food Safety and the Limits of Interpretation

The travel-time results in this article are not used to infer food-safety compliance or violation. The analysis does not measure food temperature, vehicle-cabin temperature, food holding time, or food-handling procedures. The WHO Five Keys to Safer Food manual and the SPPG food-safety certification guidance provide context that food distribution requires risk control, but the travel-time values in this study only flag potential logistical exposure that warrants further examination (World Health Organization, 2006; Badan Gizi Nasional, 2025b).

The maximum of 22.275 minutes on a depot-to-school route under the controlled-extreme scenario, then, does not indicate that operations breach food safety. What it does say is narrower: under heavier traffic and rain, travel time can lengthen, and that lengthening belongs among the design considerations for thermal control, distribution scheduling, and service SOPs.

H. Limitations

Several limits bound how far these results should be pushed. On the data side, the school records stand in as simulative service nodes with no official MBG/SPPG status, the student counts are a service proxy rather than real portion figures, and the TomTom readings are a ten-point pilot snapshot of the segments around each monitoring point, not a multi-day profile, and not the end-to-end time of any full OD route. On the assumptions, the weather state at TomTom retrieval was not independently verified, which creates the double-counting risk that leads us to label S_5 a conservative upper bound and to report the non-composite comparator $\max(\alpha, \beta)$; the baseline speed $v_0 = 30$ km/h and the weather multipliers $1.05/1.10/1.20$ are assumed rather than calibrated for Medan, and because a constant-speed model can under-predict real travel time (Boeing & Zhou, 2026), the absolute S_1 values should be read as indicative, while the weather factor is applied homogeneously across the network even though rain's effect varies with ponding, drainage, elevation, and traffic density, and the OSM network has not been validated against official local road data. In scope, the model does not yet include vehicle capacity, service times, school reception schedules, actual route ordering, or field validation. Future work should therefore pursue direct empirical validation, for example comparing the estimates against real vehicle-trip data or an independent routing service on selected routes, calibrate v_0 and β against pilot data, and add multi-day traffic data, vehicle departure and arrival times, food-temperature data, vehicle capacities, and a route-optimization model.

4. CONCLUSION

This article produces a data-driven travel-time scenario framework to support the preliminary analysis of school meal distribution as part of education-support logistics. The framework integrates depot and school node data, a road-network distance matrix from OSMnx, pilot TomTom traffic observations, and historical Open-Meteo weather profiles.

The mathematical contribution lies in transforming road-network distance L_{ij} into scenario travel-time estimates T_{ij}^h through the parameters v_0, α_h, β_h, and θ_h. The model places the depot-to-school result as the primary metric because it matches the service context of distribution from a single depot to schools. The all-OD-pairs statistic is still reported as a secondary network reading.

The main results show the mean depot-to-school travel time rising from 7.766 minutes under the normal scenario to 13.908 minutes under the controlled-extreme scenario, while the non-composite comparator $\max(\alpha, \beta)$ places S_5 at 12.644 minutes; we interpret this range as a conservative upper bound. The depot-to-school P90 increases from 11.044 to 19.779 minutes. On the all-OD statistic, mean travel time rises from 9.935 to 17.793 minutes, while P90 increases from 15.763 to 28.230 minutes. The sensitivity analysis shows that uncertainty in the baseline speed v_0 produces a proportional and opposite change in travel time ($\varepsilon_{v_0} = -1$) within the scalar model used here.

We position the framework as an early computational representation, not as final route optimization, an operational validation of SPPG, a food-safety model, or an operational digital twin, and it occupies an explicitly earlier stage than existing school-meal route-optimization work (Gajpal *et al*., 2019; World Food Programme Innovation Accelerator, 2026). Subsequent research should add multi-day traffic data, actual vehicle arrival times, vehicle capacities, school service times, food-temperature conditions, parameter calibration, and a route-optimization model, so that the analysis can move from an early scenario toward firmer operational decision-making.

ACKNOWLEDGEMENTS

This research was funded by the PNBP (Non-Tax State Revenue) of Universitas Negeri Medan for the 2026 fiscal year under Rector's Decree No. 0236/UN33/KPT/2026. We are grateful to the OpenStreetMap contributors, OSMnx, TomTom, and Open-Meteo, whose freely shared resources made this work possible.

REFERENCES

Acharya, S., Garikapati, V. M., Allen, M., Lyu, M., Hoehne, C., Sharda, S., & Fitzgerald, R. (2024). Enriching OpenStreetMap network data for transportation applications: Insights into the impact of urban congestion on accessibility. *Journal of Transport Geography*, 104096. https://doi.org/10.1016/j.jtrangeo.2024.104096

Badan Gizi Nasional. (2025a). *Petunjuk teknis tata kelola penyelenggaraan Program Makan Bergizi Gratis Tahun Anggaran 2026* (Keputusan Kepala Badan Gizi Nasional Republik Indonesia Nomor 401.1 Tahun 2025, ditetapkan 29 Desember 2025). Badan Gizi Nasional Republik Indonesia. https://www.bgn.go.id/juknis/lB1PKg-petunjuk-teknis-tata-kelola-penyelenggaraan-program-makan-bergizi-gratis

Badan Gizi Nasional. (2025b). *Pedoman sertifikasi keamanan pangan pada Satuan Pelayanan Pemenuhan Gizi* (Keputusan Kepala Badan Gizi Nasional Republik Indonesia Nomor 52.2 Tahun 2025). Badan Gizi Nasional Republik Indonesia. https://www.bgn.go.id/juknis/xEm8Jv-pedoman-sertifikasi-keamanan-pangan-pada-satuan-pelayanan-pemenuhan-gizi

Badan Gizi Nasional. (2026, May 31). *Sejak 6 Januari 2025-29 Mei 2026, 8.182 SPPG pernah di-suspend, 2.213 SPPG kini masih dalam posisi suspend* [Press release]. Badan Gizi Nasional Republik Indonesia. https://www.bgn.go.id/news/siaran-pers/sejak-6-januari-2025-29-mei-2026-8182-sppg-pernah-di-suspend-2213-sppg-kini-masih-dalam-posisi-suspend

Blauth, J., Held, S., Müller, D., Schlomberg, N., Traub, V., & Tröbst, T. (2022). *Vehicle routing with time-dependent travel times: Theory, practice, and benchmarks*. arXiv. https://doi.org/10.48550/arXiv.2205.00889

Bliznashka, L., Blakstad, M. M., Berhane, Y., Ismail, A., & Fawzi, W. W. (2024). School feeding for improving child nutrition in conflict-affected settings: Feasibility and cost efficiency of alternative models in Yemen. *Annals of the New York Academy of Sciences*, 1540(1), 251–264. https://doi.org/10.1111/nyas.15222

Boeing, G. (2017). OSMnx: New methods for acquiring, constructing, analyzing, and visualizing complex street networks. *Computers, Environment and Urban Systems*, 65, 126-139. https://doi.org/10.1016/j.compenvurbsys.2017.05.004

Boeing, G. (2022). Street network models and indicators for every urban area in the world. *Geographical Analysis*, 54(3), 519-535. https://doi.org/10.1111/gean.12281

Boeing, G. (2025). Modeling and analyzing urban networks and amenities with OSMnx. *Geographical Analysis*, 57(4), 567-577. https://doi.org/10.1111/gean.70009

Boeing, G., & Zhou, Y. (2026). Travel time prediction from sparse open data. *International Journal of Geographical Information Science*. Advance online publication. https://doi.org/10.1080/13658816.2026.2628193

Bundy, D., de Silva, N., Horton, S., Jamison, D. T., & Patton, G. C. (Eds.). (2017). *Disease Control Priorities: Child and Adolescent Health and Development* (3rd ed., Vol. 8). World Bank. https://doi.org/10.1596/978-1-4648-0423-6

Cohen, J. F. W., Jahn, J. L., Richardson, S., Cluggish, S. A., Parker, E., & Rimm, E. B. (2016). Amount of time to eat lunch is associated with children's selection and consumption of school meal entrée, fruits, vegetables, and milk. *Journal of the Academy of Nutrition and Dietetics*, 116(1), 123-128. https://doi.org/10.1016/j.jand.2015.07.019

Cools, M., Moons, E., & Wets, G. (2010). Assessing the impact of weather on traffic intensity. *Weather, Climate, and Society*, 2(1), 60-68. https://doi.org/10.1175/2009WCAS1014.1

Drake, L., Woolnough, A., Burbano, C., & Bundy, D. (Eds.). (2016). *Global School Feeding Sourcebook: Lessons from 14 Countries*. Imperial College Press.

Gajpal, Y., Roy, V., & Sahay, B. S. (2019). Vehicle routing for a mid-day meal delivery distribution system. *Heliyon*, 5(2), e01158. https://doi.org/10.1016/j.heliyon.2019.e01158

Gendreau, M., Ghiani, G., & Guerriero, E. (2015). Time-dependent routing problems: A review. *Computers & Operations Research*, 64, 189-197. https://doi.org/10.1016/j.cor.2015.06.001

Huber, S., & Rust, C. (2016). Calculate travel time and distance with OpenStreetMap data using the Open Source Routing Machine (OSRM). *The Stata Journal*, 16(2), 416-423. https://doi.org/10.1177/1536867X1601600209

Ichoua, S., Gendreau, M., & Potvin, J.-Y. (2003). Vehicle dispatching with time-dependent travel times. *European Journal of Operational Research*, 144(2), 379-396. https://doi.org/10.1016/S0377-2217(02)00147-9

Ludwig, C., Psotta, J., Buch, A., Kolaxidis, N., Fendrich, S., Zia, M., Fürle, J., Rousell, A., & Zipf, A. (2023). Traffic speed modelling to improve travel time estimation in openrouteservice. *The International Archives* *of the Photogrammetry, Remote Sensing and Spatial Information Sciences, XLVIII-4/W7-2023*, 109–116. https://doi.org/10.5194/isprs-archives-XLVIII-4-W7-2023-109-2023

Malandraki, C., & Daskin, M. S. (1992). Time dependent vehicle routing problems: Formulations, properties and heuristic algorithms. *Transportation Science*, 26(3), 185-200. https://doi.org/10.1287/trsc.26.3.185

Maze, T. H., Agarwal, M., & Burchett, G. (2006). Whether weather matters to traffic demand, traffic safety, and traffic operations and flow. *Transportation Research Record*, 1948(1), 170-176. https://doi.org/10.3141/1948-19

Open-Meteo. (2026). *Historical Weather API documentation*. Open-Meteo. Retrieved 2026, from https://open-meteo.com/en/docs/historical-weather-api

Sakhare, R. S., Zhang, Y., Li, H., & Bullock, D. M. (2023). Impact of rain intensity on interstate traffic speeds using connected vehicle data. *Vehicles*, 5(1), 133–155. https://doi.org/10.3390/vehicles5010009

TomTom. (2025). *Flow Segment Data: Traffic API documentation*. TomTom Developer Portal. https://developer.tomtom.com/traffic-api/documentation/tomtom-maps/v1/traffic-flow/flow-segment-data

Tsapakis, I., Cheng, T., & Bolbol, A. (2013). Impact of weather conditions on macroscopic urban travel times. *Journal of Transport Geography*, 28, 204-211. https://doi.org/10.1016/j.jtrangeo.2012.11.003

Wang, D., Shinde, S., Young, T., & Fawzi, W. W. (2021). Impacts of school feeding on educational and health outcomes of school-age children and adolescents in low- and middle-income countries: A systematic review and meta-analysis. *Journal of Global Health*, 11, 04051. https://doi.org/10.7189/jogh.11.04051

World Food Programme Innovation Accelerator. (2026). *Route the Meals: Optimizing delivery networks and routes for efficient humanitarian supply chains*. World Food Programme. Retrieved 2026, from https://innovation.wfp.org/project/route-meals

World Health Organization. (2006). *Five keys to safer food manual*. World Health Organization. https://www.who.int/publications/i/item/9789241594639

Xiong, M.-M., Han, Z.-Y., Lu, B., Guo, J., Xu, S., Yang, Y.-J., & Huang, H. (2022). Effects of rainfall on the weekday traffic flow in major cities of the Beijing–Tianjin–Hebei region, China, in 2021. *Advances in Climate Change Research*, 13(6), 858–867. https://doi.org/10.1016/j.accre.2022.11.009